Journal of Solid State Chemistry 182 (2009) 841–848

Contents lists available at ScienceDirect

Journal of Solid State Chemistry

journal homepage: www.elsevier.com/locate/jssc

Structure variation and luminescence properties of lanthanide complexes with 1,9-bis [2-(2′-picolylaminoformyl)-1,4,7,9-tetraoxadecane

Xue-Qin Song [a,b], Zhi-Peng Zang [a], Wei-Sheng Liu [a,*], Yu-Jie Zhang [b]

[a] College of Chemistry and Chemical Engineering and State Key Laboratory of Applied Organic Chemistry, Lanzhou University, Lanzhou 730000, China
[b] School of Chemical and Biological Engineering, Lanzhou Jiaotong University, Lanzhou 730070, China

ARTICLE INFO

Article history:
Received 27 September 2008
Received in revised form
19 December 2008
Accepted 29 December 2008
Available online 6 January 2009

Keywords:
Salicylamide
Lanthanide complex
Supramolecular structure
Luminescence properties

ABSTRACT

Using 1,9-salicylamide bissubstituted oxadecane ligand, 1,9-bis [2-(2′-picolylaminoformyl)-1,4,7,9-tetraoxadecane (L), two novel lanthanide complexes have been prepared and well characterized by means of elemental analysis, IR spectroscopy, UV–vis spectroscopy, TGA analysis and single-crystal X-ray diffraction. $\{[PrL(NO_3)_3(H_2O)_2]\cdot CH_3OH\}_n$ is a 1D zigzag polymer with three-dimensional supramolecular structure formed by hydrogen bonds, while $[EuL(NO_3)_3(H_2O)]_n$ is a linear coordination polymer and present an interesting supramolecular double chain, which are very different from the structure of terbium complex reported before. The result reported herein demonstrated that steric crowding associated with the decreasing lanthanide ion radius causes changes of the conformation of the ligand as well as structures. Luminescence studies for the Eu(III) complexes demonstrated that the salicylamide ligand also exhibits a good antennae effect for the Eu(III) ion due to efficient intersystem crossing and ligand-to-metal energy transfer and the Eu(III) ion is well shielded from the surrounding environment.

1. Introduction

Synthesis of luminescent lanthanide complexes has been of considerable interest because of their potential applications, such as fluorescent labeling reagents, imaging agents and emitter materials in organic light-emitting diodes (OLEDs) [1–3]. Generally, complexes of Eu(III) and Tb(III) are considered to have the brightest emission, but the luminescence efficiency of their complexes largely depends on the choice of organic ligands [4]. Since the Laporte-forbidden *f–f* transitions make direct photo-excitation of lanthanide ions unfavored, the organic ligands function like an antenna by absorbing light and transferring this energy to the excited states of the central lanthanide ion. The excited lanthanide ion then undergoes radiative transitions to lower energy states resulting in characteristic multiple narrow-band emissions. Since the intensity of the emission (brightness) and choice of lanthanide (i.e., color of emission) both depend on the sensitizer, new sensitizing chromophores are highly sought after [5].

Owing to the structural features of salicylamide derivatives, their lanthanide complexes have some advantages for luminescence research: (1) the high extinction coefficients of these ligands in the near ultraviolet–visible range provide effective absorption of excitation energy, which promotes more effective energy transfer to the lanthanide ion; (2) they hold flexibility because of the presence of a $-NHCH_2-$ spacer between the aromatic ring as well as flexible backbone in some cases that may bend to require its conformation to coordinate to metal centers; (3) the presence of O and N atoms and aromatic rings may form hydrogen bonds and $\pi-\pi$ stacking interactions, to extend and stabilize the whole framework series. As a result, several fascinating supramolecular structure resulted [6–9]. Acyclic polyethers offer many advantages in the extraction and analysis (ion selective electrodes) of lanthanides. Their ring-like coordination structures and terminal group effects on the extractability have been widely studied [10,11]. A survey of the literature on salicylamide substituted acyclic polyether bridged lanthanide complexes revealed that, to date, crystal structure and luminescent studies on Ln(III) (Ln denotes a generic member of the lanthanide series) complexes were scarce [12].

The radii of the Ln cations decrease with increasing atomic number, which imposes evident influences on the coordination geometry and might lead to different types of structure and physical properties. Thus, it was interesting to examine whether the architecture is maintained across the Ln. To date, only few reports are concerned with the diversity of Ln-based structures controlled by the radii of Ln ions [8,13–19]. With the aim of investigating such an interesting area, we have now extended our studies of the ligand, 1,9-bis [2-(2′-picolylaminoformyl)-1,4,7,9-tetraoxadecane (L) (Scheme 1) both on the diversity

* Corresponding author. Fax: +86 9318912582.
E-mail address: liuws@lzu.edu.cn (W.-S. Liu).

0022-4596/$ - see front matter © 2009 Published by Elsevier Inc.
doi:10.1016/j.jssc.2008.12.025

supramolecular structure and on the luminescence properties of the Eu(III) complex.

2. Experimental

2.1. Materials

The commercially available chemicals were of A.R. grade and were used without further purification.

2.2. Methods

The metal ions were determined by EDTA titration using xylenol orange as indicator. Carbon, Nitrogen and Hydrogen analyses were performed using an EL elemental analyzer. Thermogravimetric analyses (TGA) were performed with a WCT-2A thermoanalyzer under air atmosphere (30–700 °C) at a heating rate of 10 °C/min. IR spectroscopy (4000–400 cm^{-1}) were obtained with KBr discs on a Therrno Mattson FTIR spectrometer. ^1H NMR spectroscopy were recorded on a Brucker DRX 300 spectrometer in $CDCl_3$ solution with TMS as internal standard. Electronic spectroscopy were recorded with a Varian Cary 100 spectrophotometer in ethyl acetate solution. Fluorescence measurements were made on FLS920 of Edinburgh Instrument equipped with quartz curettes of 1 cm path length with a xenon lamp as the excitation source. An excitation and emission slit of 2.5 nm were used for the measurements of luminescence in solid state. Quantum yields were determined by an absolute method using an integrating sphere on FLS920 of Edinburgh Instrument. The luminescence decays were recorded using a pumped dye laser (Lambda Physics model FL2002) as the excitation source. The nominal pulse width and the linewidth of the dye-laser output were 10 ns and 0.18 cm^{-1}, respectively. The emission of a sample was collected by two lenses into a monochromator (WDG30), detected by a photomultiplier and processed by a Boxcar Average (EGG model 162) in line with a microcomputer. Reported luminescence lifetimes are averages of at least three independent determinations.

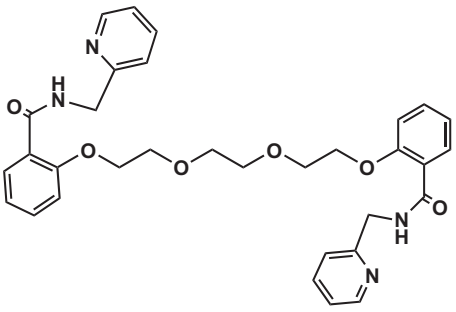

Scheme 1. The schematic illustration of ligand L.

2.3. Crystal structure determination

Suitable single crystal of the nitrate complex was carefully selected under an optical microscope and subsequently glued to the tip of a glass fiber. Intensity data were collected on a Bruker SMART 1000 CCD diffractometer using Mo$K\alpha$ radiation ($\lambda = 0.71073$ Å) and integrated using the SAINT suite of software. The absorption corrections were calculated using SADABS. Primary non-hydrogen atoms were solved by direct method and refined anisotropically by full-matrix least-squares methods on F^2. Hydrogen atoms were placed in calculated positions and included in the final cycles of refinement using a riding model. The programs for structure solution and refinement were SHELXS-97 and SHELXL-97, respectively [20]. The crystal data and refinement results are summarized in Table 1. Selected bond lengths and angles are given in Tables 2 and 3 respectively.

CCDC reference numbers 644769 and 702811.

2.4. Synthesis of the ligand

The ligand was synthesized and characterized as reported in literature [12].

2.5. Syntheses of the complexes

General procedure for the synthesis of lanthanide complexes was reported before [12].

Table 1
Crystal data and structure refinement for Pr(III) and Eu(III) complex.

Empirical formula	C_{33} H_{42} N_7 O_{18} Pr	C_{32} H_{36} Eu N_7 O_{16}
Formula weight	965.65	926.64
Temperature (K)	298(2)	298(2)
Wavelength (Å)	0.71073	0.71073
Crystal system, space group	Monoclinic, $P2(1)/c$	Triclinic, $P-1$
Unit cell dimensions	$a = 8.873(2)$ Å, $\alpha = 90°$	$a = 11.5827(11)$ Å, $\alpha = 70.2560(10)°$
	$b = 23.623(3)$ Å, $\beta = 97.620(2)°$	$b = 12.5041(13)$ Å, $\beta = 69.9580(10)°$
	$c = 19.567(3)$ Å, $\gamma = 90°$	$c = 14.8118(18)$ Å, $\gamma = 88.632(2)°$
Volume (Å^3)	4064.8(12)	1886.6(4)
Z, Calculated density (kg/m^3)	4, 1.578	2, 1.631
Absorption coefficient (mm^{-1})	1.282	1.744
F(000)	1968	936
Crystal size (mm)	$0.37 \times 0.17 \times 0.13$	$0.36 \times 0.30 \times 0.18$
Theta range for data collection (°)	1.36–25.01	1.56–25.01
Limiting indices	$-10 \leqslant h \leqslant 10$, $-24 \leqslant k \leqslant 28$, $-18 \leqslant l \leqslant 23$	$-13 \leqslant h \leqslant 11$, $-14 \leqslant k \leqslant 14$, $-17 \leqslant l \leqslant 13$
Reflections collected/unique	16581/7121 [R(int) = 0.0588]	9888/6548 [R(int) = 0.0156]
Completeness to theta = 25.01	99.2%	98.5%
Absorption correction	Semi-empirical from equivalents	Semi-empirical from equivalents
Max. and min. transmission	0.8510 and 0.6484	0.8510 and 0.6484
Refinement method	Full-matrix least-squares on F^2	Full-matrix least-squares on F^2
Data/restraints/parameters	7121/184/533	6548/0/505
Goodness-of-fit on F^2	1.043	1.078
Final R indices [$I > 2$sigma(I)]	$R1 = 0.0627$, w$R2 = 0.1363$	$R1 = 0.0264$, w$R2 = 0.0578$
R indices (all data)	$R1 = 0.1043$, w$R2 = 0.1552$	$R1 = 0.0353$, w$R2 = 0.0632$
Largest diff. peak and hole (e. Å^{-3})	1.268 and −1.321	0.936 and −0.546

Table 2
Selected bond lengths (Å) and angles (°) for $\{[PrL(NO_3)_3(H_2O)_2]\cdot CH_3OH\}_n$ complex.

Pr(1)–O(6) 2.429(5)		Pr(1)–O(5) 2.436(5)		Pr(1)–O(17) 2.503(5)	Pr(1)–O(16) 2.517(5)
Pr(1)–O(10) 2.574(5)		Pr(1)–O(13) 2.578(5)		Pr(1)–O(14) 2.607(6)	Pr(1)–O(11) 2.615(5)
Pr(1)–O(8) 2.557(5)		Pr(1)–O(7) 2.709(5)			
O(6)–Pr(1)–O(5)	77.20(17)	O(6)–Pr(1)–O(17)	75.77(17)	O(5)–Pr(1)–O(17)	77.90(18)
O(5)–Pr(1)–O(16)	73.34(17)	O(17)–Pr(1)–O(16)	149.42(18)	O(6)–Pr(1)–O(8)	159.05(18)
O(17)–Pr(1)–O(8)	114.27(18)	O(16)–Pr(1)–O(8)	74.59(19)	O(6)–Pr(1)–O(10)	116.83(17)
O(17)–Pr(1)–O(10)	136.52(18)	O(16)–Pr(1)–O(10)	73.93(18)	O(8)–Pr(1)–O(10)	69.58(18)
O(5)–Pr(1)–O(13)	130.34(18)	O(17)–Pr(1)–O(13)	70.89(18)	O(16)–Pr(1)–O(13)	137.42(18)
O(10)–Pr(1)–O(13)	69.53(18)	O(6)–Pr(1)–O(14)	82.56(17)	O(5)–Pr(1)–O(14)	145.69(19)
O(16)–Pr(1)–O(14)	133.56(18)	O(8)–Pr(1)–O(14)	117.79(19)	O(10)–Pr(1)–O(14)	70.54(19)
O(6)–Pr(1)–O(11)	68.35(17)	O(5)–Pr(1)–O(11)	128.96(17)	O(17)–Pr(1)–O(11)	125.24(18)
O(8)–Pr(1)–O(11)	113.94(19)	O(13)–Pr(1)–O(11)	100.66(18)	O(14)–Pr(1)–O(11)	65.25(19)
O(5)–Pr(1)–O(7)	68.44(18)	O(17)–Pr(1)–O(7)	67.18(18)	O(13)–Pr(1)–O(7)	64.24(18)
O(8)–Pr(1)–O(7)	47.95(18)	O(10)–Pr(1)–O(11)	48.55(17)	O(10)–Pr(1)–O(7)	109.47(18)
O(14)–Pr(1)–O(7)	109.10(18)	O(11)–Pr(1)–O(7)	157.93(18)	O(6)–Pr(1)–O(16)	87.79(18)
O(5)–Pr(1)–O(8)	86.78(18)	O(5)–Pr(1)–O(10)	143.64(19)	O(6)–Pr(1)–O(13)	128.04(18)
O(8)–Pr(1)–O(13)	72.77(18)	O(17)–Pr(1)–O(14)	70.37(18)	O(13)–Pr(1)–O(14)	49.31(17)
O(16)–Pr(1)–O(11)	68.96(18)	O(6)–Pr(1)–O(7)	133.41(18)	O(16)–Pr(1)–O(7)	110.32(18)

Table 3
Selected bond lengths (Å) and angles (°) for $[EuL(NO_3)_3(H_2O)]_n$ complex.

Eu(1)–O(5)	2.317(2)	Eu(1)–O(6)	2.345(2)	Eu(1)–O(16)	2.422(2)	Eu(1)–O(7)	2.435(2)
Eu(1)–O(14)	2.474(2)	Eu(1)–O(13)	2.476(2)	Eu(1)–O(11)	2.479(2)	Eu(1)–O(8)	2.552(2)
Eu(1)–O(10)	2.562(2)						
O(5)–Eu(1)–O(6)	148.60(9)		O(5)–Eu(1)–O(16)	140.54(9)		O(6)–Eu(1)–O(16)	70.78(7)
O(5)–Eu(1)–O(7)	92.82(9)		O(6)–Eu(1)–O(7)	84.65(8)		O(16)–Eu(1)–O(7)	88.15(8)
O(5)–Eu(1)–O(14)	78.93(8)		O(6)–Eu(1)–O(14)	76.58(8)		O(16)–Eu(1)–O(14)	131.65(8)
O(7)–Eu(1)–O(14)	123.49(8)		O(5)–Eu(1)–O(13)	73.99(9)		O(6)–Eu(1)–O(13)	75.50(8)
O(16)–Eu(1)–O(13	142.17(8)		O(7)–Eu(1)–O(13)	71.93(9)		O(14)–Eu(1)–O(13)	51.93(8)
O(5)–Eu(1)–O(11)	96.85(9)		O(6)–Eu(1)–O(11)	92.15(8)		O(16)–Eu(1)–O(11)	78.05(9)
O(7)–Eu(1)–O(11)	166.12(9)		O(14)–Eu(1)–O(11)	68.44(8)		O(13)–Eu(1)–O(11)	120.36(8)
O(5)–Eu(1)–O(8)	78.88(9)		O(6)–Eu(1)–O(8)	120.96(8)		O(16)–Eu(1)–O(8)	71.54(8)
O(7)–Eu(1)–O(8)	50.52(8)		O(14)–Eu(1)–O(8)	156.56(9)		O(13)–Eu(1)–O(8)	113.93(8)
O(11)–Eu(1)–O(8)	121.86(8)		O(5)–Eu(1)–O(10)	75.86(9)		O(6)–Eu(1)–O(10)	130.78(8)
O(16)–Eu(1)–O(10)	71.00(8)		O(7)–Eu(1)–O(10)	123.60(8)		O(14)–Eu(1)–O(10)	108.43(8)
O(13)–Eu(1)–O(10)	146.72(9)		O(11)–Eu(1)–O(10)	50.27(8)		O(8)–Eu(1)–O(10)	73.10(8)

$\{[PrL(NO_3)_3(H_2O)_2]\cdot CH_3OH\}_n$ Yield 42%. Anal. found (%): C, 41.13; H, 4.36; N, 10.20; Pr, 14.53. Calcd for $C_{33}H_{42}N_7O_{18}Pr$ (%): C, 41.05; H, 4.38; N, 10.15; Pr, 14.59. Major IR bands (KBr; ν, cm^{-1}): 3352 (broad, m), 2924(m), 1611 (s, C=O), 1562 (s), 1483 (s), 1450 (s), 1309 (s), 1236 (s), 1110 (m), 1038 (m), 755 (m). $[EuL(NO_3)_3(H_2O)]_n$ Yield 48%. Anal. found (%): C, 41.43; H, 3.94; N, 10.53; Eu, 16.43. Calcd for $C_{32}H_{36}EuN_7O_{16}$ (%): C, 41.48; H, 3.92; N, 10.58; Er, 16.40. Major IR bands (KBr; ν, cm^{-1}): 1611 (s, C=O), 1589(w), 1569(w), 1446(s), 1394(w), 1276(w), 1230(s), 1215(s), 1146(s), 1108(s), 1088(vs), 996(w), 855(s), 842(s), 822(w), 772 (s), 750(w), 726(w), 637(s), 626(s), 577(s), 557(w), 527(w).

3. Results and discussion

3.1. Thermal studies

The TG curves for $\{[PrL(NO_3)_3(H_2O)_2]\cdot CH_3OH\}_n$ and $[EuL(NO_3)_3(H_2O)]_n$ exhibit several mass loss steps, although without a clear plateau. The first observed mass loss takes place below 150 °C, attributed to dehydration plus demethanolation for $\{[PrL(NO_3)_3(H_2O)_2]\cdot CH_3OH\}_n$ and dehydration process for $[EuL(NO_3)_3(H_2O)]_n$. The next mass losses, correspond to the combustion of the organic moieties. The overall weight loss was 80.2% for Pr(III) complex and 79.7% for Eu(III) complex, which are in relatively good agreement with the calculated values, 82.4% and 81.0%, respectively. The X-ray powder diffraction pattern of the decomposition product obtained at 600 °C gave diffraction peaks corresponding to Pr_6O_{11}, Eu_2O_3 and some other minor peaks belonging to unknown compound(s), respectively.

3.2. Physical measurements

The new complexes gave satisfactory microanalytical results, justifying its purity. Analytical data for the complexes conform to a 1:1 (metal:L) stoichiometry. All the complexes are soluble in DMSO, DMF, CH_3OH, C_2H_5OH, acetone and slightly soluble in CH_3CN and ethyl acetate.

The IR spectrum of the free L shows bands at 1649, 1251 and 1133 cm^{-1}, which may be assigned to ν(C=O) and ν(C–O–C), respectively. In the IR spectroscopy of the Pr(III) and Eu(III) complex, the band of ether group remains almost unchanged, but the band for the carbonyl group red shifts to about 1611 cm^{-1} ($\nu = 38\ cm^{-1}$) as compared to the free ligand, thus indicating that only the oxygen atoms of the carbonyl group take part in coordination to the lanthanide ion. The general pattern of the IR spectroscopy supports the normal coordination of the bidentate nitrate group. The IR spectroscopy for the complexes contains broad bands between 3353 and 3433 cm^{-1} due to the asymmetric and symmetric O–H stretching vibrations of the hydration water molecule(s). The band at about 1592 cm^{-1} due to the hydrogening bonding for Tb(III) compex is not present in the IR spectrum of Pr(III) and Eu(III) complex confirming the absence of free carbonyl groups in these two compounds.

3.3. Crystal structure descriptions

$\{[PrL(NO_3)_3(H_2O)_2]\cdot CH_3OH\}_n$ The structure comprises of a covalently bonded one-dimensional (1D) zigzag chain of composition $[Pr(NO_3)_3L(H_2O)_2]_n$ crystallized in the monoclinic $P2_1/n$ space group which is quite different from the structure of Tb(III) complex [12]. As shown in Fig. 1, each Pr(III) node lies in a distorted bicapped square antiprism coordination sphere, which is defined by two carbonyl oxygen, six nitrate oxygen and two aquo oxygen donors with Pr–O distances range from 2.557(5) to 2.709(5) Å. The two carbonyl oxygens of the same ligand are coordinated to the two different Pr(III) ion in a trans configuration and the ligand coordinates to the Pr(III) as a bidentate ligand which is unambiguously different from that of Tb(III) complex [12]. It is noteworthy to comment on the distribution of functional groups about the Pr(III) center: the three bidentate nitrate groups have an approximately orthogonal arrangement on one side of the Pr center, whereas two carbonyl linkages as well as two water molecules arranged on the opposite side. The presence of only one crystallographically unique Pr site in alternate 180° arrangements, leads to the bonding of bridging O5 and O6 with other O5 and O6, respectively, giving rise to the zigzag nature of the [001] chain (Fig. 2) with a Pr–Pr–Pr internal angle of 85.21°. The Pr···Pr separations linked by the same bridging ligand are ca. 18.18 Å and the separations between alternate Pr(III) centers (on the same side of the zig-zag) are at ca. 24.61 Å.

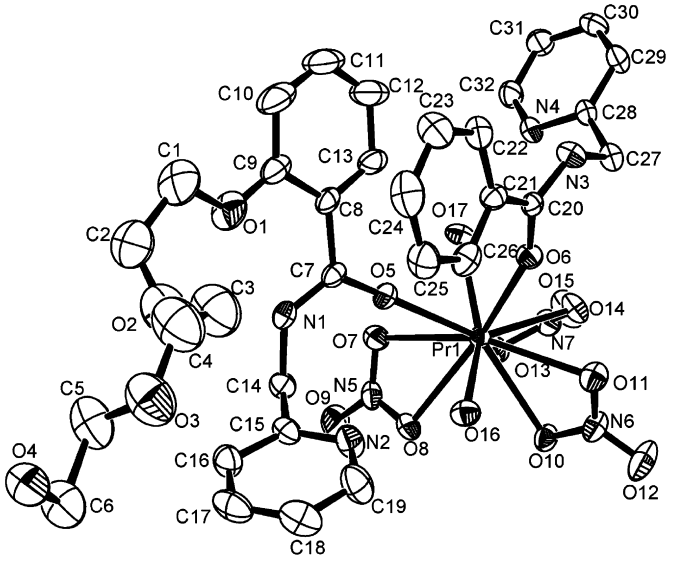

Fig. 1. ORTEP plot of complex $\{[PrL(NO_3)_3(H_2O)_2]\cdot CH_3OH\}_n$ showing the local coordination environment of Pr(III) with thermal ellipsoids at 30% probability (crystalline solvent molecules as well as hydrogen atoms are omitted for clarity).

In the context of inorganic crystal engineering, the combination of coordination chemistry with non-covalent interactions, such as hydrogen bonding, provides a powerful method for generating supramolecular architectures from simple building blocks [21–24]. Both types of connections are valuable for the design of network solids since they are directional interactions. The hydrogen atoms attached to the amide nitrogen atoms have the ability to form donor hydrogen bonds. This kind of non-covalent bond has the potential to assemble smaller, simpler fragments into the desired cavities under favorable conditions, which is important in host–guest chemistry and has applications in chemistry, biology and materials science [25]. Moreover, by using coordination polymers instead of discrete complexes as tectons, the resulting structures have fewer degrees of freedom, which facilitate structural prediction and control.

The oxygen atoms of the nitrate anions (O9) act as H-bond acceptors while the amide nitrogen atoms (N1) act as donors, constitute complementary hydrogen bonding recognition sites on the backbone of the 1D coordination polymer with the N···O separations of 3.031(3) Å, and N–H···O angles of 121.2(1)°, hence the formation of an interesting 2D supramolecular structure (Fig. 3). In addition, the free methanol molecule (O18) plays an important role in the structure, which links the neutral chains with two (O18···O17 2.842 (8) Å, O18···O16 2.822 (8) Å) hydrogen bond from two different directions, As a result, neutral chains are interpenetrated into a 3D supramolecular structure (Fig. 4).

There were also strong intramolecular hydrogen bonding between the amide nitrogen atoms and the etheric oxygen atoms with O···N separations ca. 2.61 Å, and N–H···O angles averaging 137° as well as pyridyl nitrogen atom and water oxygen atom with O···N separations ca. 2.74 Å, N–H···O angles averaging 148° within Pr(III) complex. It is no doubt to note that the robust intramolecular hydrogen bond have a template effect and participate in the stabilization of the complete architecture.

$[EuL(NO_3)_3(H_2O)]_n$ Once the ligand coordinated with Eu(III), the coordination environment of the metal ions changes dramatically and the coordination number decreases from 10 to 9. The difference may be ascribed to the larger ionic radius and less electronic density of Pr(III) compared to Eu(III), which allows a higher coordination number for the former. As shown in Fig. 5, the asymmetric unit contains one Eu(III) ion and two half ligands (from two crystallographically independent ligands) such that all Eu(III) ions are crystallographically equivalent. The europium complex of the ligand crystallizes in the monoclinic $P-1$ space group. The coordination polyhedron around the Eu(III) ion is

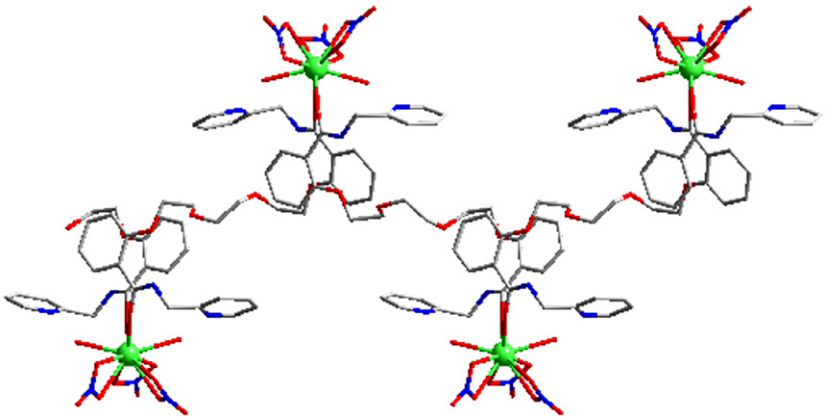

Fig. 2. 1D coordination polymer chain of Pr(III) complex (crystalline solvent molecules and hydrogen atoms are omitted for clarity).

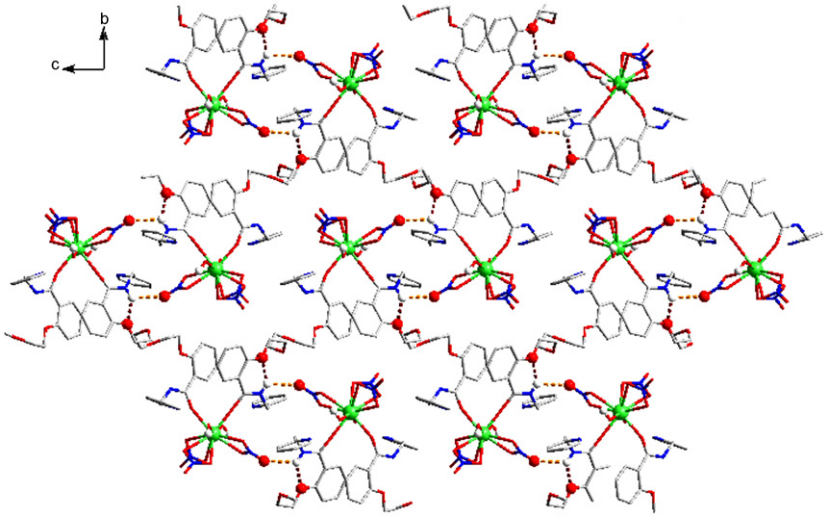

Fig. 3. The 2D supramolecular structure of Pr(III) complex constructed by hydrogen bonding between coordinated nitrate ion and amide nitrogen atoms as well as that of etheric oxygen and amide nitrogen atoms which are indicated with orange and brown dashed lines. (hydrogen atoms except those for hydrogening bonding are omitted for clarity).

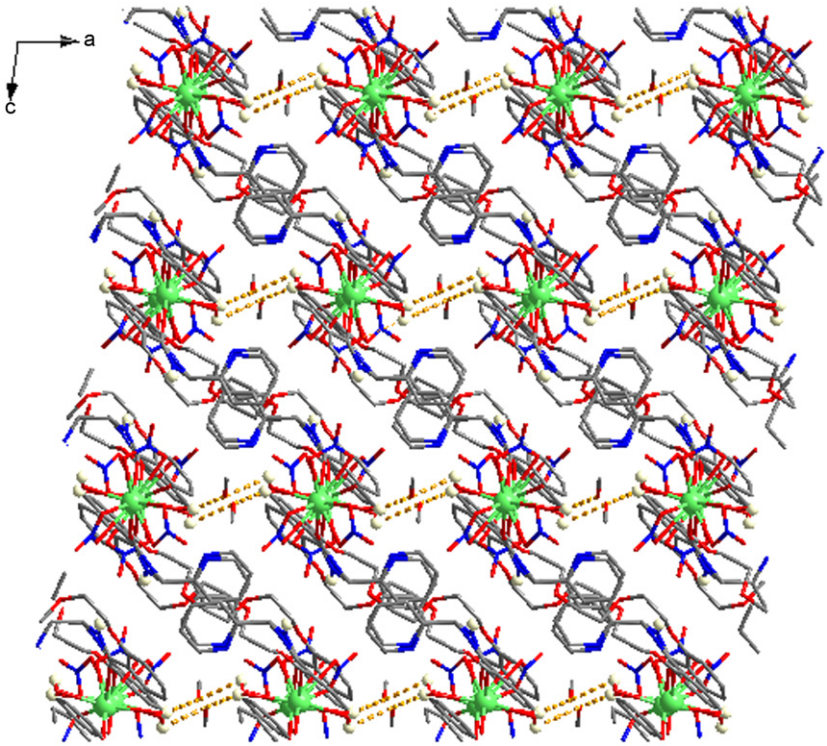

Fig. 4. The 3D supramolecular structure of Pr(III) complex constructed by hydrogen bonding (hydrogen atoms except those for hydrogening bonding are omitted for clarity).

distorted, monocapped anti-square prism. There is one water molecule and three bidentate nitrate anions completing the nine-coordinate sphere of europium ion, and the distances to the water molecule oxygen atom is Eu–O(16) 2.422(2) Å. The other oxygen atoms are at distances between 2.317(2) and 2.562(2) Å. The ligand coordinate in a bidentate bridging mode with the ligand in a trans configuration which is similar to that of Pr(III) complex. This arrangement of two ligands around the europium ion leads to a ⋯Eu⋯L⋯Eu⋯L⋯ linear chain (Fig. 6) with the Eu⋯Eu separations linked by the same bridging ligand at ca. 16.84 Å. As shown in Fig. 7, the adjacent chains are connected through strong O–H⋯O hydrogen bonds with an O16⋯O12 distance of 2.900 Å and O16–H16B⋯O12 angle of 159.3° which extend the 1D chains into a double-chain supramolecular structure. It is obvious that the robust intramolecular hydrogen bond have a template effect and participate in the stabilization of the complete architecture just like those in supramolecular structure of Pr(III) and Tb(III) complex.

Many lanthanide complexes based on the same ligand usually have alike building blocks due to similar valence shell electron configurations [26]. However, polymers constructed from Pr(III), Eu(III) and mononuclear Tb(III) complex with the ligand present

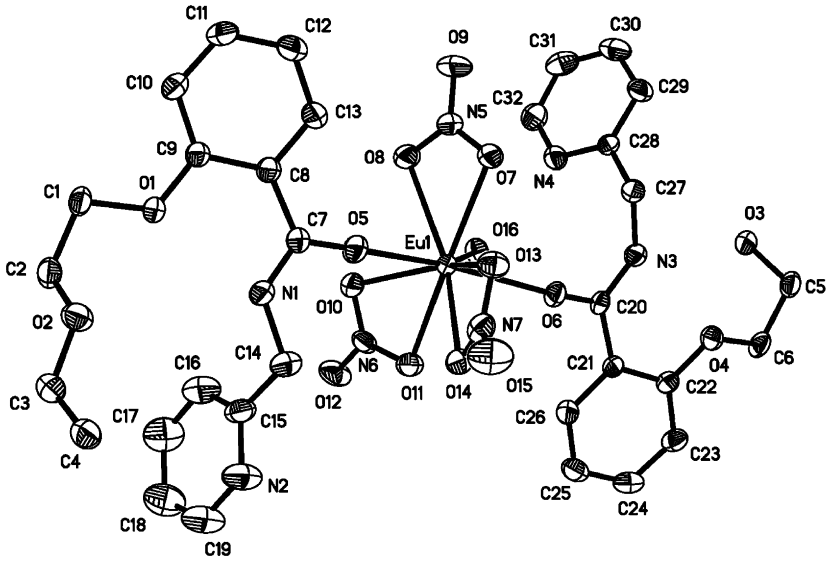

Fig. 5. ORTEP plot of complex $[EuL(NO_3)_3(H_2O)]_n$ showing the local coordination environment of Eu(III) with thermal ellipsoids at 30% probability (hydrogen atoms are omitted for clarity).

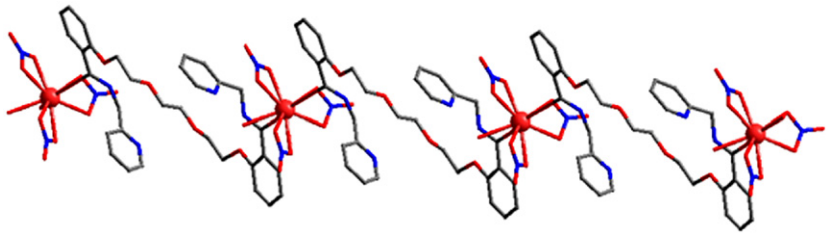

Fig. 6. 1D coordination polymer chain of Eu(III) complex (hydrogen atoms are omitted for clarity).

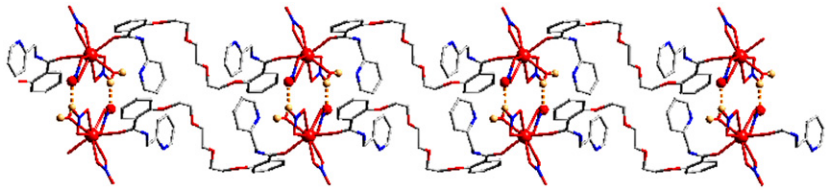

Fig. 7. The double-chain supramolecular structure constructed by hydrogen bonding between coordinated water and nitrate oxygen atoms which are indicated with orange dashed lines. (hydrogen atoms except those for hydrogening bonding are omitted for clarity).

different arrays. The possible explanation for this change might be the combination of the versatile coordinative behavior of the ligand and the templating effect resulting from the different lanthanide ions due to all the complex crystallized under exactly the same conditions, such as solvent system, temperature, concentration, metal-to-ligand ratio. The ligand conformation in these coordination polymers contracts due to the lanthanide contraction effect. It is important to note that the etheric oxygen atoms of the two ligands are not coordinated to Ln(III) center, but act as the hydrogen bonding acceptors to form strong intramolecular N–H···O hydrogen bonds which are stabilized by a stable six-membered ring. The binding of lanthanide ions to the carbonyl oxygen atoms of ligands rather than to etheric oxygen groups appears largely as a consequence of cooperative effect of strong intramolecular hydrogen bonds and the steric hinderance inhibiting the formation of a reasonable coordination geometry that involves the participation of all four ether oxygen donors of each ligand. In any case, a number of etheric oxygen-containing amide ligands have been documented previously [27] to exhibit strong affinities for lanthanide.

3.4. Photophysical properties of the ligand

In acetonitrile, the absorption spectroscopy of the ligand L (Fig. 8) features three main bands located around 203 (ε/dm^3 mol^{-1} cm^{-1}, 26250), 230 (ε/dm^3 mol^{-1} cm^{-1}, 9650) and 287 nm (ε/dm^3 mol^{-1} cm^{-1}, 2825) with the tail of the band extending to 308 nm. The bands could be assigned to characteristic π–π^* transitions centered on benzene, pyridine ring and the salicylamide units, respectively. The titration of Ln^{3+} was also carried out by adding aliquots of $Ln(NO_3)_3$ acetonitrile solution into the acetonitrile solutions containing ligands L. Upon the addition of a $Eu(NO_3)_3 \cdot 6H_2O$ acetonitrile solution, the absorption band of 203 nm increases to a limit value with moderate bathochromic shift, the band of 234 nm gets unconspicuous and

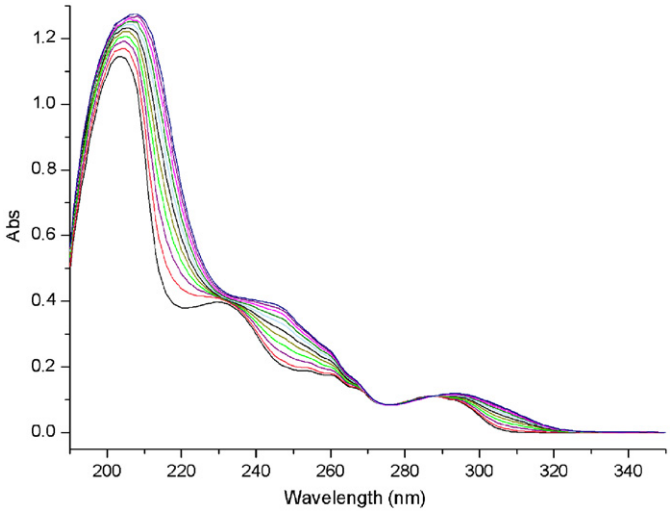

Fig. 8. UV–vis titration profile of ligand L (4×10^{-5} M) in acetonitrile solution upon addition of Eu(III) nitrate.

replaced by a shoulder, and the band at 287 nm only shows a moderate bathochromic shift with the tail of the band extending to ca. 320 nm. The obvious changes during the titration in the UV–vis spectrum suggest significant change in the overall electronic structure of the ligands upon addition of Eu^{3+}, which is quite different from those reported by us before [8,9]. In addition the large molar absorption coefficient of the ligands indicates favorable conditions for an efficient antenna effect. Excited by the absorption band at 305 nm, the ligands display strong luminescence band around 341 and 447 nm. The ligand-centered luminescence in the Gd(III) complex displays basically the same features observed in the free ligand, thus confirming the suitability of this ligand as a sensitizer for Eu(III) and Tb(III) luminescence.

3.5. *Luminescence properties of the the Eu(III) complex in the solid state*

The excitation spectrum of Eu(III) complex shown in Fig. 9 was collected by monitoring the Eu(III) emission band at 580 nm. The spectrum consists of several sharp bands overlaying on a dominant broad band that covers the high-energy side of the spectrum. The bands at 397, 416 and 465 nm are sharp *f–f* transitions characteristic of the Eu(III) ion, which correspond to transitions from the ground $^7F_0$ level to the $^5L_6$, $^5D_3$ and $^5D_2$ states, respectively [28]. The dominant broad band, which is centered at 312 nm, is uncharacteristic of *f–f* transitions. Comparison of the complex's absorption spectrum and the excitation profile of Eu(III) complex indicates that the excitation maximum appears at the tail of the complex absorption band. Observation of characteristic Eu(III) emission lines upon excitation into this broad band unambiguously demonstrates that the sensitized emission is achieved through antenna triplet states.

The luminescence spectroscopy of Eu(III) complex displays metal-centered line emissions as shown in Fig. 10. The $^5D_0\rightarrow{}^7F_0$ transition shows a well-defined single peak at 580 nm, while the $^5D_0\rightarrow{}^7F_1$ region has a broader band at 592 nm. The $^5D_0\rightarrow{}^7F_2$ region displays the most intense but weakly resolved band at 616 nm with a shoulder at its half intensity. Weak bands are also observed at ~691 and 703 nm corresponding to $^5D_0\rightarrow{}^7F_4$ transitions. Notably, the $^5D_0\rightarrow{}^7F_2$ transition is much more intense than the $^5D_0\rightarrow{}^7F_1$ transition, the large intensity ratio of Eu(III) complex for $I(^5D_0\rightarrow{}^7F_2)/I(^5D_0\rightarrow{}^7F_1)$ indicates the lower symmetric coordination environment at the Eu(III) site which is in agreement with the result of single-crystal X-ray analysis [29]. The fluorescence quantum yield Φ of the europium nitrate complex in solid state was found to be $4.7\pm0.1\%$ using an integrating sphere. The Eu(III) complex luminescence decay is best described by a single-exponential process with significantly longer lifetimes of $\tau1=1.637\pm0.001$ ms, indicating the presence of one distinct emitting species. For the comparison purpose, we measured the lifetime and quantum yield in the 77 K, both the lifetime τ and the fluorescence quantum yield Φ of the europium nitrate complex in solid state were increased to be 1.637 ± 0.001 ms and $16.4\pm0.1\%$, respectively, indicating the non-radiative transitions due to the OH oscillators in the Eu(III) first coordination shell was restrained to some extent at the low temperature.

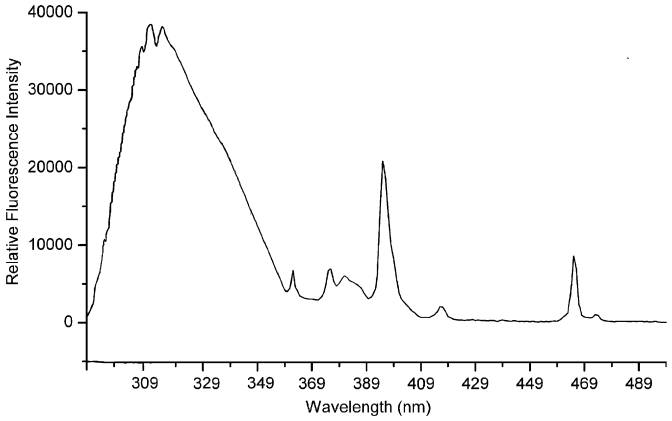

Fig. 9. Room-temperature excitation spectroscopy for Eu(III) complex of ligand L in solid state (λem = 580 nm, excitation and emission passes = 2.5 nm).

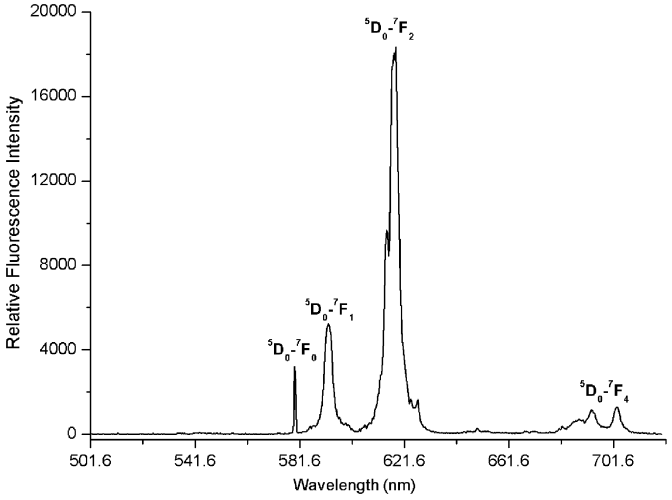

Fig. 10. Room-temperature emission spectroscopy for Eu(III) complex of ligand L in solid state (λex = 305 nm, excitation and emission passes = 2.5 nm).

4. Conclusion

In summary, fascinating supramolecular structures dependent upon both the binding-site environment of the 1,9-salicylamide bissubstituted oxadecane ligand and the nature of the metal ion have been identified. It is worth noting the result reported herein adds new merits to the chemistry of salicylamide derivatives, which are usually used as the chromophore for the lanthanide fluorescence and constituents for tunable supramolecular

chemistry. From a more general perspective, the coupling of polymer and luminescence in a material has interesting prospects for the development of luminescence materials.

5. Supplementary material

Crystallographic data for the structural analysis have been deposited with the Cambridge Crystallographic Data Center, CCDC nos. 644769 and 702811. Copies of this information may be obtained free of charge from the director, CCDC, 12 Union Road, Cambridge CB2 IEZ, UK (e-mail: deposit@ccdc.cam.ac.uk or www: http://www.ccdc.cam.ac.uk).

Acknowledgments

The authors acknowledge support from the National Natural Science Foundation of China Research (Grants 20771048, 20431010, 20621091 and J0630962).

References

[1] J.C. Frias, G. Bobba, M.J. Cann, C.J. Hutchinson, D. Parker, Org. Biomol. Chem. 1 (2003) 905.
[2] M.A. Diaz-Garcia, S.F. De Avila, M.G. Kuzyk, Appl. Phys. Lett. 81 (2002) 3924.
[3] J.-P. Duan, P.-P. Sun, C.-H. Cheng, J. Mater. Online 1 (2005).
[4] G.A. Crosby, R.E. Whan, J.J. Freeman, J. Phys. Chem. 66 (1962) 2493.
[5] S. Pope, B.J. Coe, S. Faulkner, E.V. Bichenkova, X. Yu, K.T. Douglas, J. Am. Chem. Soc. 126 (2004) 9490.
[6] J. Zhang, Y. Tang, N. Tang, M.-Y. Tan, W.-S. Liu, K.-B. Yu, J. Chem. Soc. Dalton Trans. (2002) 832.
[7] Y. Tang, J. Zhang, W.-S. Liu, M.-Y. Tan, K.-B. Yu, Polyhedron 24 (2005) 1160.
[8] X.-Q. Song, W.-S. Liu, W. Dou, Y.-W. Wang, J.-R. Zheng, Z.-P. Zang, Eur. J. Inorg. Chem. 11 (2007) 1901.
[9] X.-Q. Song, W.-S. Liu, W. Dou, J.-R. Zheng, X.-L. Tang, H.-R. Zhang, D.-Q. Wang, Dalton Trans. 27 (2008) 3582.
[10] S.X. Liu, W.S. Liu, M.Y. Tan, K.B. Yu, G.Z. Tan, Helv. Chim. Acta 80 (1997) 586.
[11] L.Y. Fan, W.S. Liu, X.M. Gan, N. Tang, M.Y. Tan, W.H. Jiang, K.B. Yu, Polyhedron 19 (2000) 779.
[12] X.-Q. Song, W. Dou, W.-S. Liu, J.-N. Yao, Y.-L. Guo, X.-L. Tang, Inorg. Chem. Commun. 10 (2007) 1058.
[13] L. Pan, X. Huang, J. Li, Y. Wu, N. Zheng, Angew. Chem. Int. Ed. 39 (2000) 527.
[14] A. Dimos, D. Tsaousis, A. Michaelides, S. Skoulika, S. Golhen, L. Ouahab, C. Didierjean, A. Aubry, Chem. Mater. 14 (2002) 2616.
[15] Q. Liu, S. Gao, J. Li, B. Ma, Q. Zhou, K. Yu, Polyhedron 21 (2002) 1097.
[16] S. Mizukami, H. Houjou, M. Kanesato, K. Hiratani, Chem. Eur. J. 9 (2003) 1521.
[17] Z. He, E. Gao, Z. Wang, C. Yan, M. Kurmoo, Inorg. Chem. 44 (2005) 862.
[18] W. Shi, X. Chen, Y. Zhao, B. Zhao, P. Cheng, A. Yu, H. Song, H. Wang, D. Liao, S. Yan, Z. Jiang, Chem. Eur. J. 11 (2005) 5031.
[19] J.-W. Cheng, S.-T. Zheng, G.-Y. Yang, Dalton Trans. (2007) 4059.
[20] [a] G.M. Sheldrick, SHELXL-97, Program for the Solution of Crystal Structures, University of Göttingen, Göttingen, Germany, 1997;
[b] G.M. Sheldrick, SHELXL-97, Program for the Refinement of Crystal Structures, University of Göttingen, Göttingen, Germany, 1997.
[21] [a] L. Brammer, J.C.M. Rivas, R. Atencio, S. Fang, F.C. Pigge, J. Chem. Soc. Dalton Trans. (2000) 3855;
[b] L. Brammer, Chem. Soc. Rev. 33 (2004) 476.
[22] [a] C.B. Aakeröy, A.M. Beatty, Aust. J. Chem. 54 (2001) 409;
[b] A.M. Beatty, Coord. Chem. Rev. 246 (2003) 131.
[23] D. Braga, Chem. Commun. (2003) 2751.
[24] T.J. Burchell, D.J. Eisler, R.J. Puddephatt, Chem. Commun. (2004) 944.
[25] [a] J. De Mendoza, Chem. Eur. J. 4 (1998) 1373;
[b] J. Rebek Jr., Acc. Chem. Res. 32 (1999) 278;
[c] L.R. MacGillivray, J.L. Atwood, Angew. Chem. Int. Ed. 38 (1999) 1018.
[26] [a] J.-R. Li, X.-H. Bu, R.-H. Zhang, C.-Y. Duan, K.M.-C. Wong, V.W.-W. Yam, New. J. Chem. 28 (2004) 261;
[b] G.M. Davies, R.J. Aarons, G.R. Motson, J.C. Jeffery, H. Adams, S. Faulkner, M.D. Ward, Dalton Trans. (2004) 1136;
[c] Z. Wang, C.-M. Jin, T. Shao, Y.-Z. Li, K.-L. Zhang, H.-T. Zhang, X.-Z. You, Inorg. Chem. Commun. 5 (2002) 642;
[d] B.D. Chandler, D.T. Cramb, G.K.H. Shimizu, J. Am. Chem. Soc. 128 (2006) 10403.
[27] [a] Y.-L. Guo, W. Dou, W.-S. Liu, D.-Q. Wang, Polyhedron 26 (2007) 1699;
[b] Y.-W. Wang, W.-S. Liu, K.-B. Yu, Anorg. Allg. Chem. 632 (2006) 482;
[c] K.-Z. Tang, J. Zhang, Y. Tang, W.-S. Liu, M.-Y. Tan, Y.-X. Sun, Inorg. Chim. Acta 8 (2005) 1018;
[d] K.-W. Lei, W.-S. Liu, M.-Y. Tan, Spectrochim. Acta Part A 66 (2007) 118;
[e] K. Matloka, A. Gelis, M. Regalbuto, G. Vandegriftb, M.J. Scott, Dalton Trans. (2005) 3719;
[f] X.F. Li, W.S. Liu, Z.J. Guo, M.Y. Tan, Inorg. Chem. 42 (2003) 8735.
[28] M. Albin, R.R. Wright Jr., W.D. Horrochs, Inorg. Chem. 24 (1985) 2491.
[29] W.S. Liu, M.Y. Tan, X. Wang, S.Y. Zhang, Acta Chimi. Sin. 48 (1990) 1090.